UCLA

UCLA Electronic Theses and Dissertations

Title

Harmonic Analysis of Limit-Cycle Oscillations Induced by Optical Injection to a Semiconductor Laser

Permalink

https://escholarship.org/uc/item/1rp4634d

Author

Lin, Chun-Ju

Publication Date

2014

Peer reviewed|Thesis/dissertation

UNIVERSITY OF CALIFORNIA

Los Angeles

Harmonic Analysis of Limit-Cycle Oscillations

Induced by Optical Injection to a Semiconductor Laser

A thesis submitted in partial satisfaction

of the requirements for the degree Master of Science

in Electrical Engineering

by

Chun-Ju Lin

2014

ABSTRACT OF THE THESIS

Harmonic Analysis of Limit-Cycle Oscillations Induced by

Optical Injection to a Semiconductor Laser

by

Chun-Ju Lin

Master of Science in Electrical Engineering

University of California, Los Angeles, 2014

Professor Jia-Ming Liu, Chair

Analysis of the limit-cycle, also known as period-one (P1), dynamics induced by strong optical injection to a semiconductor laser is carried out. Based on the well-established laser rate equations, an approximate solution of the P1 dynamics can be obtained by starting with a general limit-cycle solution. Our results are in good agreement with numerical and experimental results by taking the second harmonic of the P1 frequency into account. Our analysis shows that the strong coupling between the oscillating carrier density and the oscillating optical field is responsible for the high nonlinearity of these P1 dynamics.

The thesis of Chun-Ju Lin is approved.

_____

Chandra J. Joshi

_____

Oscar Stafsudd

_____

Jia-Ming Liu, Committee Chair

University of California, Los Angeles

2014

Table of Contents

List of Figures

List of Tables

Acknowledgements

I would like to offer my sincere appreciation for the learning opportunity provided by my committee: Professor Chandrashekar Joshi, Professor Oscar Stafsudd and Professor Jia-Ming Liu, my committee chair. I cannot express enough thanks to Professor Jia-Ming Liu, for his encouragement, continued mentoring and insightful guidance.

I would like to thank for all the help and support from my classmates in Photonics Research Laboratory. I wish to thank Mohammad for his advice, friendship and time spent on our discussions and experiments. I wish to thank Danny, Apple and Tiwen for their friendship and encouragement.

To my parents and sister, I deeply appreciate your support and love. Thank you for giving me strength for this achievement. Finally, to my caring and supportive girlfriend Chien-Jung, I offer my deepest gratitude. It was a great comfort to have your encouragement when in the tough times. It is my fortune to have you in my life.

Chapter 1

Introduction

1.1 Introduction

Semiconductor laser dynamics are easily invoked by an external perturbation. For instance, nonlinear dynamics induced by optical injection, optical feedback and optoelectronic feedback have been demonstrated [1, 2, 3, 4, 5, 6, 7, 8, 9, 10, 11, 12]. Among them, the optical injection is favorable because it can be precisely controlled to effectively induce numerous types of dynamics. These dynamics, such as stable-locking, periodic oscillation, quasi-periodic motion and chaos, are all intensively studied [7, 9, 10, 12, 13, 14, 15, 16, 17, 18, 19, 20, 21, 22, 23, 24, 25, 26, 27, 28]. In particular, the period-one (P1) oscillations induced by the optical injection have attracted considerable attention because of their unique characteristics for many

applications. The advantages of such P1 oscillations include that the system can be simple, free from complicated circuitry, and easily controlled by the operational parameters. These operational parameters usually are the injection strength, the detuning frequency, and the bias current. The injection strength refers to the normalized optical field amplitude from the master laser to the slave laser. The detuning frequency is the difference between free-running frequency of the master and the slave lasers. The P1 oscillations induced and controlled by optical injection of semiconductor lasers have been demonstrated with many important applications such as photonic microwave generator, amplitude modulation to frequency modulation (AM-FM) converter, and lidar [29, 30, 31, 32, 33]. A detailed study of these P1 dynamics is therefore desired for designing and characterizing such systems.

All the aforementioned dynamics can be predicted by numerically solving the well-established rate equations [11, 27, 34]. Also, there is much work established on the qualitative approach such as bifurcation analysis that gives the macroscopic view of the dynamics [25, 35]. However, due to the nonlinear behavior of these dynamics, the exact analytical solution cannot be quantitatively characterized. Recently, a two-frequency approximation of the P1 oscillation has been reported [36]. The two dominant frequency components are assumed to be in the steady state, and the detuning frequency and the P1 frequency are used as input parameters. When the slave laser is injected by the master laser with a relatively high injection strength and a positive

detuning frequency that is higher than its free-running relaxation resonance frequency, the

system is less nonlinear and the two-frequency approximation is in good agreement with the

numerical simulation result. Nevertheless, such approach is not valid when the detuning

frequency is on the same order or lower than the free-running relaxation resonance frequency

because the system becomes highly nonlinear in this region. Not only the deviation from the

numerical simulation result grows as the detuning frequency is reduced, but the existence of

multiple solutions also arises when the P1 frequency is used as an input to derive the

corresponding injection strength. Without numerical simulation, the detailed dynamical

characteristics become unpredictable especially when the system is under the injection condition

between the chaotic region and the Hopf bifurcation line. Hence, a different approach to

analyzing the P1 dynamics is needed.

Perturbation techniques are often considered to derive an analytical solution to a nonlinear

system [9]. Generally, perturbation techniques employ the small-parameter assumption for the

perturbation toward the approximate solution. However, this assumption is not directly

applicable to the dynamics in the highly nonlinear regions. Conventional perturbation techniques

using a small-parameter perturbation include the two-timing approach and the well-known

Poincare-Lindstedt method. The latter is a widely used approach to a weakly nonlinear problem

that has a periodic solution. However, when these techniques are used to analyze the rate

equations of the optically injected laser for the P1 dynamics, it is found that the result degenerates to the four-wave mixing condition. The small-parameter assumption that attempts to decouple the rate equations significantly suppresses the nonlinearity. In other words, the traditional perturbation technique is equivalent to perturbing the four-wave mixing phase portrait, which is far from the real orbit of the P1 oscillation; thus such approach is not applicable. New methods, such as the homotopy analysis method and the variational iteration method [37, 38, 39, 40], have been proposed for solving highly nonlinear systems without using the small-parameter perturbation. Nevertheless, these methods cannot be easily implemented in a three-dimensional coupled system such as the optically injected laser due to the complicated calculation. For these reasons, a simpler approach is developed, which is based on the knowledge of the general solution of the limit cycle.

In this thesis, instead of studying the optical frequency domain, we focus on the microwave power spectrum where the P1 oscillation frequency manifests itself. An approximate solution can be acquired by examining the spectral components and the phase trajectory of the optical field found by numerically solving the rate equation model for one operating point as the initial step. Then, the general solution of the limit cycle with initial coefficients determined from the previous step is substituted into the rate equations. The conditions for balancing the coefficients of the self-consistent solutions are thus generated. With the understanding of the typical P1 orbit

and its harmonics, our result can be applied to the P1 dynamics in the highly nonlinear region with sufficient accuracy. The region where the harmonics of the P1 frequency must be taken into account is shown as the lower shaded region as illustrated in Fig. 1.1. Based on our solution, we can then further investigate the average and the oscillating terms of each field and see how they are affected by each other.

1.2 Outline of Thesis

In Chapter 2, the discussion starts from the well-established rate-equation model of semiconductor lasers under optical injection in autonomous from. It is shown that the solution of the rate equations can be analytically obtained by series expansions and exploiting the time invariance property. On the other hand, by rewriting the rate equation model in non-autonomous form, the boundary between the bounded/unbounded phase regions is derived. This boundary plays an important role in characterizing the P1 dynamics. Chapter 3 elaborates the accuracy dependence of the approximate solutions on the highest order of the harmonic terms. The application of this analytical model in the AM-FM conversion is also discussed in this chapter. Chapter 4 presents the characterization about the photon density and carrier density. This gives a better understanding to the coupling between the optical fields and the carrier density. In the final chapter, the result is summarized and concluded with the future research.
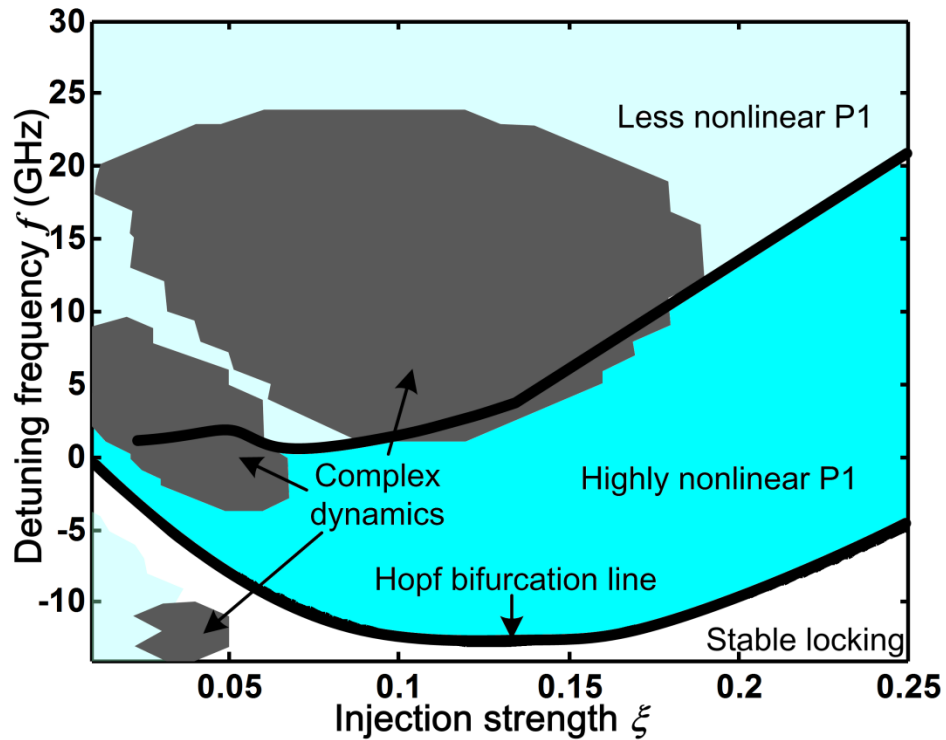
Figure 1.1: Map of dynamics of the injected laser as a function of optical injection strength and detuning frequency at $\tilde{J} = 1.222$. The lower boundary (lower thick curve) is the Hopf bifurcation line, which separates the P1 region above and the stable-locking region below. The upper boundary (upper thick line) delineates the transition line of bounded/unbounded phase P1 dynamics. Separated by this line are the less nonlinear P1 region above and the highly nonlinear P1 region below.

Chapter 2

Theoretical model

In this thesis, the analysis of the P1 dynamics of an optically injected semiconductor laser is based on the approximate solution which is derived from the well-developed rate equations in autonomous form. By inspecting the phase trajectories of the optical fields, it is shown that the P1 dynamics can be approximated by harmonic terms. In order to have enough conditions to solve for unknown coefficients, the time invariance property is exploited in the derivation. After the derivation, the three coupled nonlinear differential equations can be simplified to three algebraic equations which can be iteratively solved. On the other hand, in the region close to the Hopf bifurcation line, it is noted that more harmonic terms are needed to properly describe the P1 dynamics due to its high nonlinearity. This significantly increased nonlinearity can be related to the bounded/unbounded phase transition, which is manifest through the phase trajectories.

2.1 Coupled Rate Equations

A single-mode semiconductor laser is categorized as a class B laser because its material

polarization has a much larger relaxation rate compared to the photon and electron relaxation

rates. Hence, the laser is reduced to a two-dimensional system. With the external perturbation of

optical injection, the laser system becomes a three-dimensional system and, therefore, can have

complex nonlinear dynamics. The rate equations describing this three-dimensional system have

been previously reported, showing excellent agreement with experiment. For mathematical

simplicity, in the following analysis we use the normalized dimensionless form of the coupled

equations [41]:

$$\frac{\mathrm{d}\,x}{\mathrm{d}\,\tau} = zx + \left(bz - \hat{\Omega}\right)y + \xi,\tag{2.1}$$

$$\frac{\mathrm{d}\,y}{\mathrm{d}\,\tau} = zy - \left(bz - \hat{\Omega}\right)x,\tag{2.2}$$

$$\frac{\mathrm{d}\,z}{\mathrm{d}\,\tau} = -Az - B\left(1 + 2z\right)\left(x^2 + y^2 - 1\right).\tag{2.3}$$

The two variables x and y represent the quadrature optical field components, and z represents

the carrier density, as defined in Table 2.1. Because the optical gain provided by the carrier

density is consumed by the optical field, these three variables are coupled. The linewidth

enhancement factor, b, represents the amplitude-phase coupling of the optical field due to

changes in the carrier density. The operational parameters $\hat{\Omega}$ and ξ are the normalized detuning

frequency and the injection strength, respectively; both are defined relative to the free-running

slave laser [42]. As defined in Table 2.1, the parameters A and B in (2.3) are normalized

parameters related to the laser parameters [43]. In Table 2.1, a_r and a_i are, respectively, the real

and imaginary parts of the complex optical field; $\tilde{n}$ is the normalized carrier density; $\Omega = 2\pi f$

and $\Omega_0 = 2\pi f_0$ are the detuning frequency and the P1 frequency before normalization,

respectively; $\hat{\Omega}_0$ is the normalized P1 frequency; $\tilde{J}$ stands for the normalized bias current, γ_c for

the cavity decay rate, γ_s for the spontaneous carrier relaxation rate, and γ_n for the differential

carrier relaxation rate [44]. The value of these parameters used in the analysis are determined

experimentally for a well-studied semiconductor laser [45]: $\tilde{J} = 1.222$, $\gamma_c = 5.36\times 10^{11}$ s^{-1},

$\gamma_s = 5.96\times 10^9$ s^{-1}, $\gamma_n = 7.53\times 10^9$ s^{-1}, and $b = 3.2$. The nonlinear carrier relaxation rate γ_p [44] is

ignored in this analysis for mathematical simplicity. To account for the nonlinear gain effect, γ_p

has to be added into (2.1)-(2.3), which does not affect the validity of the approach described

below.

2.2   Solution to the Coupled Equations

The system described by (2.1)-(2.3) is autonomous. Such systems have time-invariance property.

This property can be utilized in the process of generating solutions. On the other hand, using the

autonomous equations can avoid the artificial bifurcation which exists in the non-autonomous

equations [35]. These advantages of autonomous systems are the basis of our approach.

Table 2.1
Normalized Variables and Parameters

$$x = a_r \qquad\qquad y = a_i \qquad\qquad z = \frac{\gamma_n}{2\gamma_s \tilde{J}}\tilde{n}$$

$$\tau = \gamma_c t \qquad\qquad \hat{\Omega} = \frac{\Omega}{\gamma_c} \qquad\qquad \hat{\Omega}_0 = \frac{\Omega_0}{\gamma_c}$$

$$A = \frac{(\gamma_n + \gamma_s)}{\gamma_c} \qquad\qquad B = \frac{\gamma_n}{2\gamma_c}$$

The general solution of a limit cycle can be expressed as a Fourier series [46, 47]:

$$x = x_0 + \sum_{n=1}^{m}\left(x_{no}\sin n\hat{\Omega}_0\tau + x_{ne}\cos n\hat{\Omega}_0\tau\right), \tag{2.4}$$

where x_0, x_{no}, and x_{ne} are constants, and m is an integer determined by the highest harmonic necessary to describe the limit-cycle orbit. A limit cycle that deviates more from a circular orbit requires more high-harmonic terms. The subscript o stands for the odd function, and e for the even function. Hence, x, y, and z can be expressed in this form. The conditions for the self-consistent solutions are generated by substituting the general solution into (2.1)-(2.3) and requiring both sides of each equation to be consistent. However, these conditions are not sufficient to determine all unknowns. For example, if the highest order is $m = 1$, three coefficients are to be determined for each x, y, and z. The normalized P1 frequency $\hat{\Omega}_0$ is also unknown. Therefore, there are ten unknowns whereas only nine conditions are generated for the self-consistent solution. The time-invariant property of the autonomous systems is then utilized to reduce one unknown. The time invariance allows the system status at any time to be the initial condition without changing the solution. Hence, the initial condition for the carrier density z can be assumed to be the sum of the average value z_0 and the amplitude of the cosine term z_1:

$$z\left(\tau = \tau_0\right) = z_0 + z_1 = z\left(\tau = 0\right). \tag{2.5}$$

The sine term of the carrier density is thus eliminated with this initial condition. Therefore, the

solution considering only the first harmonic of the P1 frequency can be written as

$$x = x_0 + x_{1o} \sin \hat{\Omega}_0 \tau + x_{1e} \cos \hat{\Omega}_0 \tau, \tag{2.6}$$

$$y = y_0 + y_{1o} \sin \hat{\Omega}_0 \tau + y_{1e} \cos \hat{\Omega}_0 \tau, \tag{2.7}$$

$$z = z_0 + z_1 \cos \hat{\Omega}_0 \tau, \tag{2.8}$$

where x_0 and y_0 are the average values of the normalized optical field components, (x_{1o}, y_{1o}) and (x_{1e}, y_{1e}) are the amplitudes of the sine and cosine terms of the normalized optical field components, respectively, and $\hat{\Omega}_0$ is the normalized P1 frequency to be solved. Substituting (2.6)-(2.8) into (2.1)-(2.3) results in nine equations to be solved for nine unknowns. These nine equations are the self-consistent conditions in our analysis when only the average terms and first-harmonic terms are considered by choosing $m = 1$.

The well-known cavity resonance frequency shift in the stable locking region [42, 48, 49] can be similarly defined in our model, which is simply bz_0 because γ_p is neglected. The difference between this normalized shift bz_0 and the normalized detuning frequency $\hat{\Omega}$ is then defined as $\hat{\Omega}_d$:

$$\hat{\Omega}_d = \hat{\Omega} - bz_0. \tag{2.9}$$

In the two-frequency approximation [36], this frequency difference is assumed to be the beating signal that results in the P1 frequency. This approximation is not valid in the highly nonlinear region of P1 dynamics. The P1 dynamics in this highly nonlinear region, shown as the

lower shaded region in Fig. 1.1, have sophisticated characteristics, such as low-sensitivity points

[41], that have profound implications in physics and applications. The approach described in this

thesis is valid for these highly nonlinear P1 dynamics.

By substituting (2.6)-(2.8) into (2.3), it is found that the second-harmonic components

generated by the term x^2+y^2 in (2.3) can be neglected without significant consequences. On the

other hand, by rearranging the self-consistent conditions corresponding to the oscillating optical

fields in (2.1) and (2.2), a system of linear equations can be obtained. The amplitudes of the

optical fields, which are x_{1o}, x_{1e}, y_{1o}, and y_{1e}, can thus be expressed in terms of the other variables

x_0, y_0, z_0, z_1, and $\hat{\Omega}_0$:

$$\begin{cases} x_{1o} = D^{-1}\left(1+b^2\right)\hat{\Omega}_0 z_1\left(\beta x_0 + \alpha y_0\right), \\ x_{1e} = -D^{-1}\left(1+b^2\right)z_1\left[\left(\alpha\hat{\Omega}_d + \beta z_0\right)x_0 + \left(\alpha z_0 - \beta\hat{\Omega}_d\right)y_0\right], \\ y_{1o} = D^{-1}\left(1+b^2\right)\Omega_0 z_1\left(-\alpha x_0 + \beta y_0\right), \\ y_{1e} = -D^{-1}\left(1+b^2\right)z_1\left[-\left(\alpha z_0 - \beta\hat{\Omega}_d\right)x_0 + \left(\alpha\hat{\Omega}_d + \beta z_0\right)y_0\right], \end{cases} \tag{2.10}$$

where

$$\alpha = \left(\hat{\Omega} + \hat{\Omega}_d\right)z_0 + b\left(\hat{\Omega}_0^2 - \hat{\Omega}_d^2\right), \tag{2.11}$$

$$\beta = \left(1+b^2\right)z_0^2 + \hat{\Omega}_0^2 - \hat{\Omega}^2, \tag{2.12}$$

$$D = \alpha^2 + \beta^2. \tag{2.13}$$

The two parameters α and β are defined for convenience. They are functions of $\hat{\Omega}$, z_0, and

$\hat{\Omega}_0$ only. The determinant of (2.10) is $\alpha^2 + \beta^2$ and is defined as D. It can be seen by substituting

13

(2.11) and (2.12) into (2.13) that the determinant D rapidly increases with $z_0{}^2$. In general z_0 has a negative value representing the gain deficit. When $|z_0|$ becomes large, the system degenerates to the stable-locking condition. On the other hand, when the detuning frequency Ω becomes much larger than the free-running relaxation resonance frequency Ω_r, D increases with $\hat{\Omega}$, resulting in a decreasing amplitude of the optical field oscillating at P1 frequency. The system behaves less nonlinearly in this circumstance where the P1 frequency can be described by the beating signal between the detuning frequency and the shifted cavity resonance frequency as in the two-frequency approximation. Between the stable locking and the less nonlinear P1 regions, the small D requires a large amplitude of the optical field at P1 frequency for the self-consistent solution. This is the highly nonlinear P1 region where the two-frequency approximation is not valid. It is also noted that the field amplitude is directly proportional to the oscillating carrier density. This dependence is discussed in the next chapter.

Substitution of x_{1o}, x_{1e}, y_{1o}, and y_{1e} as expressed in (2.10) into the other self-consistent conditions yields

$$
\begin{aligned}
x_0 = &-\left(z_0^2 + \hat{\Omega}_d^2\right)^{-1}\left\{D + \left(1+b^2\right)z_1^2\left(b\alpha - \beta\right) + \frac{1}{4}\left(1+b^2\right)^3 z_1^4\right\}^{-1} \\
&\times \xi\left\{Dz_0 + \frac{1}{2}\left(1+b^2\right)z_1^2\left[\left(b\alpha - \beta\right)z_0 - \left(\alpha + b\beta\right)\hat{\Omega}_d\right]\right\},
\end{aligned}
$$

(2.14)

$$y_0 = \left(z_0^2 + \hat{\Omega}_d^2\right)^{-1} \left\{ D + \left(1+b^2\right)z_1^2 \left(b\alpha - \beta\right) + \frac{1}{4}\left(1+b^2\right)^3 z_1^4 \right\}^{-1}$$

$$\times \xi \left\{ D\hat{\Omega}_d + \frac{1}{2}\left(1+b^2\right)z_1^2 \left[\left(\alpha + b\beta\right)z_0 + \left(b\alpha - \beta\right)\hat{\Omega}_d \right] \right\}, \tag{2.15}$$

$$DA - 2B\left(1+b^2\right)\left[\left(1+2z_0\right)^2 - 2z_1^2 \right]\left(\alpha\hat{\Omega}_d + \beta z_0\right)\left(x_0^2 + y_0^2\right) = 0, \tag{2.16}$$

$$D - 2B\left(1+b^2\right)\left(1+2z_0\right)\beta\left(x_0^2 + y_0^2\right) = 0, \tag{2.17}$$

$$D^2\left[A + 2B\left(x_0^2 + y_0^2 - 1\right)\right] + B\left(1+b^2\right)\left\{-2D\left(1+2z_0\right)\left(\alpha\hat{\Omega}_d + \beta z_0\right)\right.$$

$$\left. + \left(1+b^2\right)z_1^2\left[\hat{\Omega}_0^2\left(\alpha^2 + \beta^2\right) + \left(\alpha\hat{\Omega}_d + \beta z_0\right)^2 + \left(\alpha z_0 - \beta\hat{\Omega}_d\right)^2\right]\right\}\left(x_0^2 + y_0^2\right) = 0. \tag{2.18}$$

The average optical field amplitudes increase with the injection strength ξ, as seen in (2.14) and (2.15). It is also noted that the nonlinearity of (2.14) and (2.15) significantly increases with z_1. The expressions of x_0 and y_0 obtained in (2.14) and (2.15) can be further substituted into (2.16)-(2.18) such that only three unknowns z_0, z_1, and $\hat{\Omega}_0$ are left. Following the approach described above, the nine conditions for the self-consistent solution can be combined into three algebraic equations. These algebraic equations can be easily solved to find the relations among the unknowns though their solutions cannot be expressed in simple analytical forms. This approach allows us to readily introduce other parameters or effects and to derive the corresponding solution. If necessary, high-order harmonics of the P1 frequency can be included with a similar approach by choosing an integer $m > 1$ in the series expansions of the x, y, and z variables to improve the accuracy of the solution. To have a more complete model, the nonlinear

15

gain effect can also be taken into account by using a nonzero γ_{p} and a gain saturation factor b'

that might be different from the linewidth enhancement factor b [50].

2.3 The Bounded/Unbounded Phase Transition

The highlighted highly nonlinear region in Fig. 1.1 is bounded by a boundary curve derived from

the rate equations in non-autonomous form. The non-autonomous form can be obtained by

rewriting (2.1)-(2.3) as

$$a_{\mathrm{r}} + \mathrm{i}a_{\mathrm{i}} = |A_0|(1+a)\mathrm{e}^{\mathrm{i}(\Omega t + \phi)}. \tag{2.19}$$

$$\frac{da}{dt} = \frac{1}{2}\frac{\gamma_{\mathrm{c}}\gamma_{\mathrm{n}}}{\gamma_{\mathrm{s}}\tilde{J}}\tilde{n}(1+a) + \xi\gamma_{\mathrm{c}}\cos(\Omega t + \phi). \tag{2.20}$$

$$\frac{d\phi}{dt} = -\frac{b}{2}\frac{\gamma_{\mathrm{c}}\gamma_{\mathrm{n}}}{\gamma_{\mathrm{s}}\tilde{J}}\tilde{n} - \frac{\xi\gamma_{\mathrm{c}}}{1+a}\sin(\Omega t + \phi). \tag{2.21}$$

$$\frac{d\tilde{n}}{dt} = -\gamma_{\mathrm{s}}\tilde{n} - \gamma_{\mathrm{n}}(1+a)^2\tilde{n} - \gamma_{\mathrm{s}}\tilde{J}(2a + a^2). \tag{2.22}$$

where $|A_0|$ stands for the free-running intracavity field amplitude at the free-running slave laser

frequency ω_0, a for the normalized field amplitude, and ϕ for the phase difference between the

injection field and the injected laser. Equations (2.20)-(2.22) can be viewed as the result of

coordinate transformation for the system to be described in polar coordinates. It is noted that the

phase discussed in the following is the total phase difference $\Omega t + \phi(t)$ is the phase discussed in

the following. In this polar coordinate system, P1 dynamics can have bounded or unbounded

phases, and the transition between them can be considered as an artificial bifurcation [35]. The boundary curve that separates the bounded/unbounded phases also separates the highly nonlinear P1 region from the less nonlinear P1 region. It can be shown by examining the trajectories of the state variables that the concepts of the highly/less nonlinear P1 dynamics and the bounded/unbounded phases are closely related. Figure 2.1 presents the phase trajectories of a_r and a_i with the injection strength $\xi = 0.2$ and the detuning frequency from -8 GHz to 30 GHz. These injection conditions form a vertical line in the map of dynamics, which experiences the bounded/unbounded phase transition without crossing the chaos region. The highly nonlinear and less nonlinear P1 regions can be clearly identified through these conditions. As shown in Fig. 2.1(e) and (f), the less nonlinear P1 has a more circular trajectory enclosing the origin of the coordinates; thus the phase monotonically increases or decreases with time. By contrast, the highly nonlinear P1 has a bean-shaped trajectory that does not enclose the origin; thus the phase only varies in an interval so that it is bounded, as in Fig. 2.1(a)-(d). To describe this bean-shaped trajectory, more harmonics of the P1 frequency in the power spectrum are needed. For this reason, the two-frequency approximation is no longer valid in this region.

The boundary curve can be obtained from (2.21) with the understanding that the P1 dynamic with an unbounded phase has the monotonically increasing phase $\Omega t + \phi(t)$. When the transition from the unbounded phase to the bounded phase occurs, the time derivative of the phase
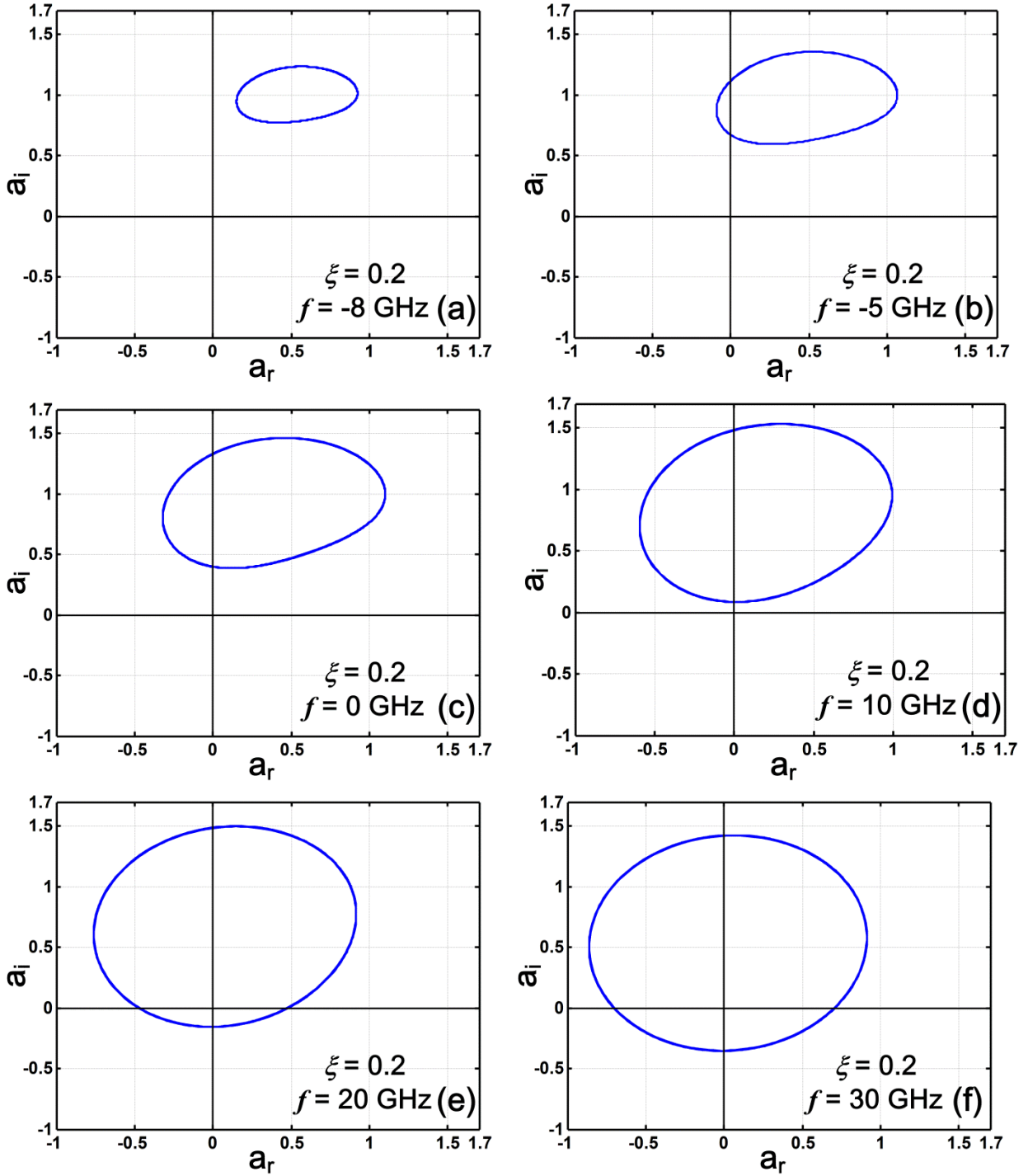
Figure 2.1: Phase trajectories of a_r and a_i at $\tilde{J} = 1.222$ with the injection strength $\xi = 0.2$ and the detuning frequency f = (a) -8 GHz, (b) -5 GHz, (c) 0 GHz, (d) 10 GHz, (e) 20 GHz, and (f) 30 GHz.

becomes zero. This signifies the change of the phase behavior such that the phase alternately increases and decreases in this bounded phase region. Because $d\phi(t)/dt$ changes with time in the P1 region, the boundary curve is obtained by requiring the minimal value of $\Omega + d\phi(t)/dt$ to be positive in the unbounded phase region, which is

$$\text{Min}\left\{\Omega - \frac{b}{2}\frac{\gamma_c \gamma_n}{\gamma_s \tilde{J}}\tilde{n}(t) - \frac{\xi\gamma_c}{1+a}\sin\left[\Omega t + \phi(t)\right]\right\} = 0. \tag{2.23}$$

As show in Fig. 1.1, the region above the higher boundary curve has the minimal value of $\Omega + d\phi/dt$ larger than zero, which indicates that the phase monotonically increases. Below this boundary curve is the bounded phase region where $\Omega + d\phi/dt$ alternately takes positive and negative values; this region is also the highly nonlinear P1 region. The system becomes more nonlinear as the operating condition moves closer to the Hopf bifurcation line because another attractor coexists [35]. Therefore, in this region close to the Hopf bifurcation line, despite the total phase of our approximate solution becomes continuously negative, such P1 dynamics is still highly nonlinear. This can also be seen from Fig. 2.1(a) and (b) that the trajectories tend to converge to one fixed point which corresponds to the stable locking fixed point.

Chapter 3

P1 Frequency Mapping

The P1 dynamics have many useful applications such as photonic microwave generator, amplitude modulation to frequency modulation (AM-FM) converter, and lidar [29, 30, 31, 32, 33]. The P1 frequency dependence on the operational parameters, including injection strength and detuning frequency, needs to be thoroughly investigated for designing such systems. However, most published work are based on the numerical simulation [11, 27, 34] or the bifurcation analysis [25, 35]. This is because of the nonlinear behavior of the P1 dynamics, which make it difficult to obtain the exact analytical solution. Although numerical simulation can give highly accurate result with high computation cost, the relation between parameters is difficult to be characterized. A two-frequency approximation of the P1 oscillation has been

reported for this purpose; however, it is only valid in the less nonlinear P1 region [36]. To show

the validity of our approximated solution, the P1 frequency mapping is present and is compared

with the results from the numerical simulation and the two-frequency approximation. The

relation between parameters can be characterized by investigating our approximated solution,

and this will be shown in the next chapter.

3.1 Introduction

The following results are obtained by using the iteration method based on the trust-region dogleg

algorithm to solve the self-consistent conditions. The dogleg method finds the step by combining

Cauchy step and Gauss-Newton step. All the parameters used in this thesis are experimentally

found by the well-known four-wave mixing technique [44]. In addition, to support the validity of

our model, the results of the numerical simulation of (2.1)-(2.3) are also presented for direct

comparison with the results obtained from the analytical approach described above. The

numerical simulation is based on the second-order Runge-Kutta method with high accuracy and

is already corroborated by many experimental results [27].

3.2 Oscillation Frequency

Figure 3.1 shows the P1 frequency maps obtained from our analysis (red squares) using series expansions of different values of m to include different numbers of harmonics: in (a), only terms up to the first harmonic are considered in the series expansions by choosing $m = 1$; in (b), terms up to the second harmonic are considered by choosing $m = 2$; in (c), terms up to the third harmonic are considered by choosing $m = 3$. For direct comparison, the results obtained by numerical simulation (black curves) are also shown. The horizontal axis represents the injection strength ξ and the vertical axis represents the detuning frequency $f = \Omega/2\pi$. The contour curves and symbols represent the P1 frequency obtained by numerical simulation and analytical iteration, respectively. The Hopf bifurcation line (thick curve) separates the P1 region above (colored) and the stable locking below (uncolored). Above the Hopf bifurcation line, the P1 dynamics covers the majority of the map, whereas two island regions surrounded by P1 dynamics represent complex dynamics such as period-doubling and chaos [23].

In Fig. 3.1(a), it can be seen that the result obtained from the analysis up to only first harmonic, though not very accurate compared to the numerical simulation result, already has a better validity over the whole map than the two-frequency approximation (open circles), which completely fails in the most nonlinear region in the lower part of the map. In particular, along the Hopf bifurcation line, our result matches the bifurcation points, whereas the two-frequency
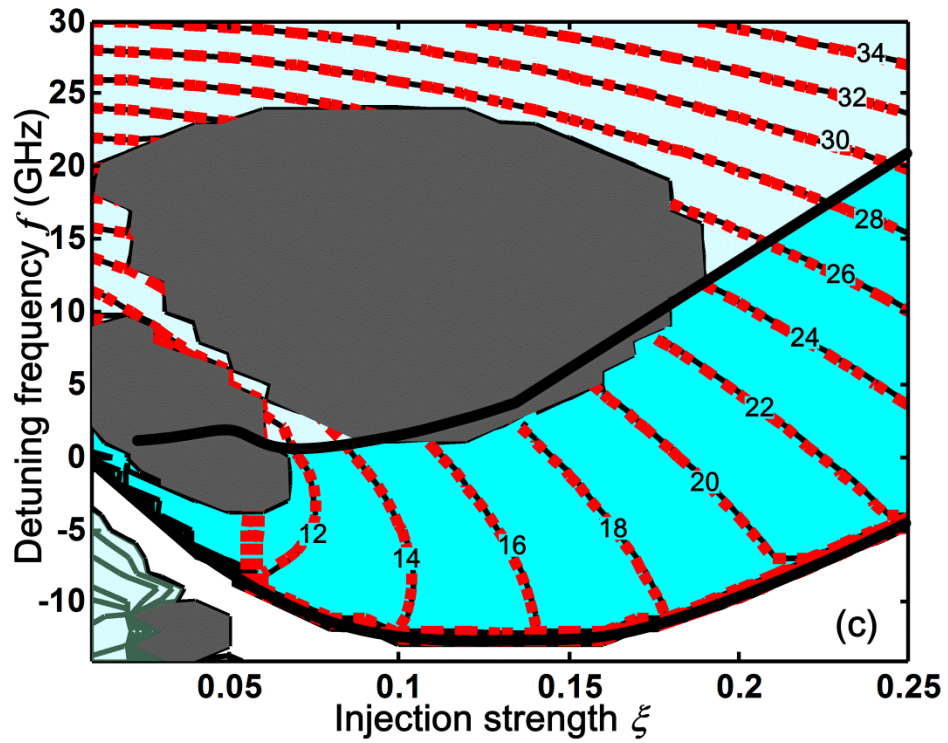
22
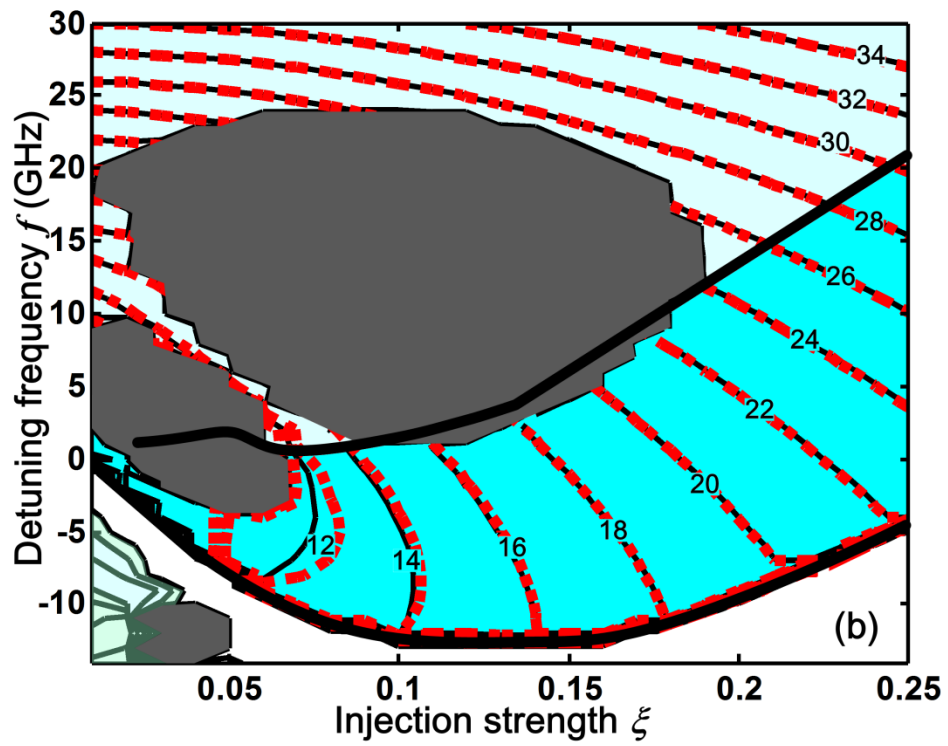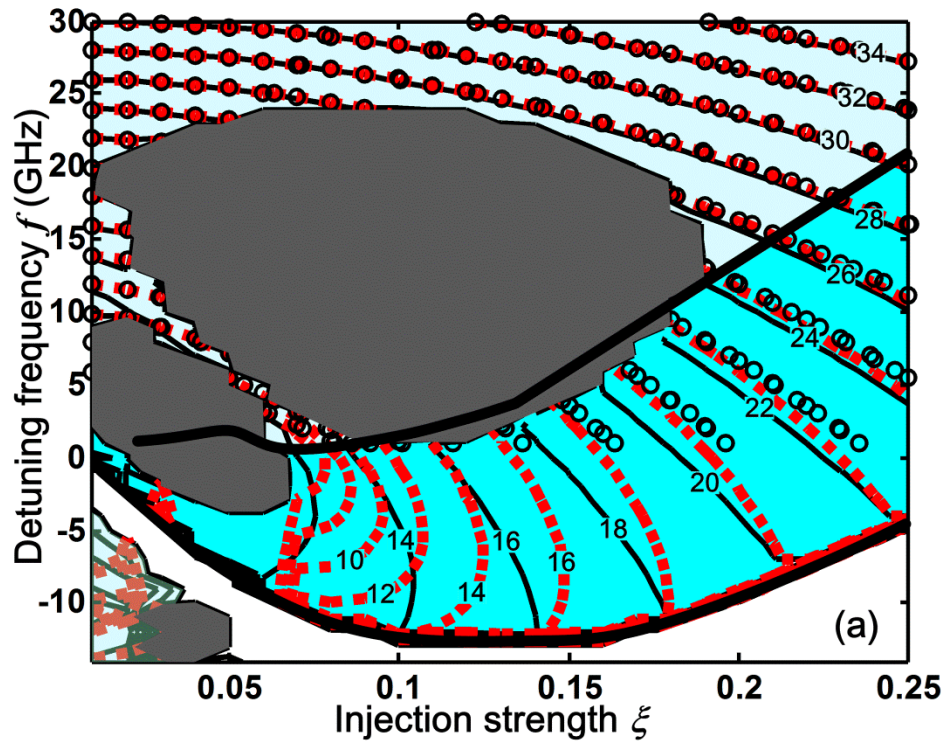
Figure 3.1 P1 frequency map as a function of optical injection strength and detuning frequency at $\tilde{J} = 1.222$. The results obtained from our analytical approach (red squares) using series expansions up to (a) first-harmonic, (b) second-harmonic, and (c) third-harmonic terms are compared to those obtained from numerical simulation (black curves). The open circles in (a) show the results from the two-frequency approximation. The boundary curves and the regions separated by them are the same as those described in Fig. 1.1.

approximation cannot predict the bifurcation points. Nevertheless, in the highly nonlinear region right above the Hopf bifurcation line, the P1 frequencies obtained from our analysis including only up to the first harmonic significantly disagree with those obtained from the numerical analysis. In addition, the upper boundary of the small region of complex dynamics above the Hopf bifurcation line characterizes the saddle-node bifurcation of limit cycles [41]; hence the assumed first-harmonic solution form is no longer adequate. The large island region corresponds to mostly period-two (P2) dynamics, which are signified by the emergence of a subharmonic frequency. Hence, the P2 dynamics do not affect the solution form. Nevertheless, the P1 frequency obtained in this region is not the fundamental frequency of a P2 dynamic. To accurately obtain the fundamental P2 frequency, the subharmonics must also be included in the self-consistent conditions. The four-wave mixing region, however, cannot be distinguished because the oscillating frequency is just the detuning frequency, which is the same as the P1 frequency in the four-wave mixing region. Therefore, there is no criterion to separate the two conditions in our model.

In the highly nonlinear region bounded by the Hopf bifurcation line below and the curve (2.23), it is necessary to include higher harmonics in our analysis to increase the accuracy of the analysis. The results obtained with $m = 2$ including the second-harmonic terms are shown in Fig. 3.1(b), and those obtained with $m = 3$ including the third-harmonic terms are shown in Fig.

3.1(c). As seen in Fig. 3.1(b), the accuracy is significantly increased by adding only the

second-harmonic terms to this analysis. Along the Hopf bifurcation line, the resonance frequency

near these bifurcation points are all identified correctly. The remaining disagreement with the

numerical simulation results occurs near the saddle-node bifurcation of limit cycles as in Fig.

3.1(a) or where a P1 frequency contour has a large curvature. It is emphasized that only the

second-harmonic terms of the optical field components x and y are considered in the analytical

results shown in Fig. 3.1(b). The second-harmonic term of the carrier density z turns out to be

negligible without causing much deviation from the numerical simulation results. This implies

that the high-order harmonics of the optical field, but not those of the carrier density, are

important in the highly nonlinear P1 region. From Fig. 3.1(c), it can be seen that the frequency

map obtained from the analysis including the terms up to the third-harmonic for the optical field

components is in excellent agreement with the numerical simulation results except in the small

region of high nonlinearity right below the saddle-node bifurcation of limit cycles. Practically,

including the second-harmonic is sufficient for a very good approximate solution except for a

small region of very high nonlinearity; therefore, the second harmonic solution is used to

generate the following results.

3.3 Dynamic Range of the P1 Frequency

The relation between the injection strength and the P1 frequency is shown in Fig. 3.2. This figure is important for its application in the AM-FM conversion [31]. Our harmonic analysis (red squares) is presented in comparison with the numerical simulation (black curves). For each model, the results from left to right correspond to the detuning frequency $f = -5$, 5, 15, and 25 GHz, respectively. The results from the harmonic analysis are in good agreement with the numerical simulation results. This plot shows the dynamic range of the P1 frequency in the practical application. The results from the two-frequency approximation are also shown for comparison (open circles). It is observed that even when the detuning frequency $f = \Omega/2\pi$ is still larger than the resonance frequency $f_r = \Omega_r/2\pi$, which is about 10 GHz, the results from the two-frequency approximation already differ significantly from the correct results because only part of the P1 oscillating field is considered in that approximation.

3.4 Summary

The dependence of the accuracy on the number of the harmonic terms is discussed in this chapter. It is shown that with up to second-harmonic terms for optical fields and up to first-harmonic terms for carrier density, the accuracy of our approximate solution is adequate for most regions in the dynamics map. Therefore, this condition is used for the following chapter. This
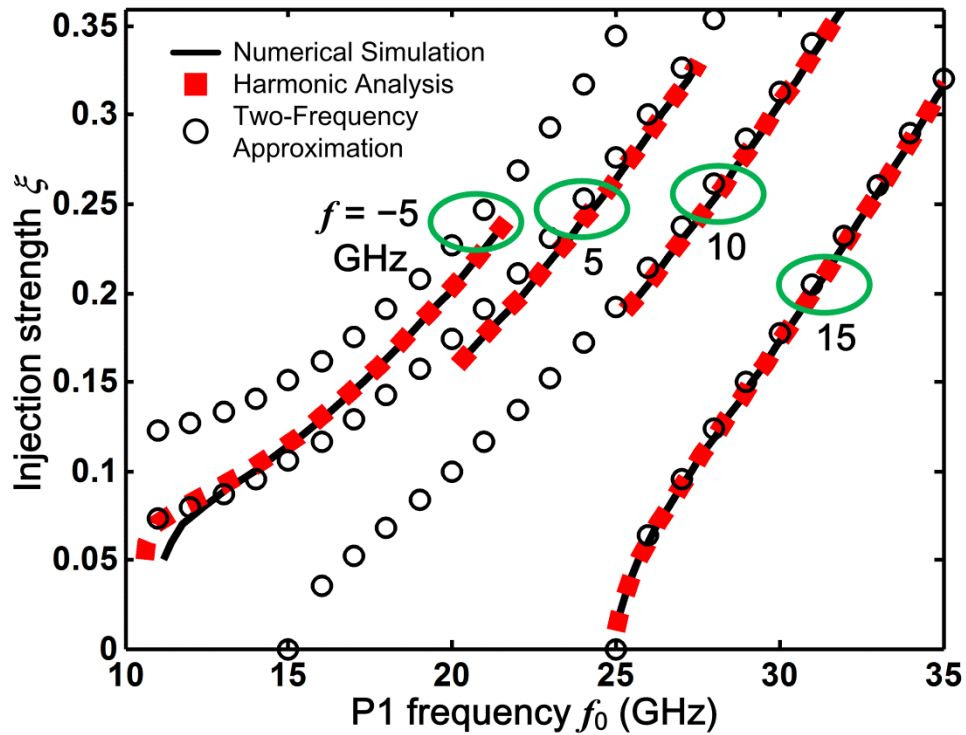
Figure 3.2: Injection strength versus P1 frequency. The black curves are from the numerical simulation, the open squares are from our harmonic analysis, and the open circles are from the two-frequency approximation. For each model, the results from left to right are obtained by setting the detuning frequency $f = \Omega/2\pi$ at -5, 5, 15, and 25 GHz, respectively.

dependence also reflects the fact that the carrier density has a more circular phase trajectory than the optical fields such that less terms are needed for this accuracy. The dynamical range of the P1 frequency for the practical application is also shown in this chapter. Our results are in excellent agreement with the numerical simulation, which implies the sufficiency of using up to second-harmonic terms for optical fields and up to first-harmonic terms for carrier density expansion.

Chapter 4

Photon Density and Carrier Density Characterization

In the process of deriving solutions, the strong coupling between the optical fields and the carrier density is shown. It is expected that the approximation solution with series expansion to $m = 2$ has similar behavior as the solution with series expansion to $m = 1$. To investigate the correlation of the optical fields and the carrier density in the solution with higher order series expansions, the same procedure is used to solve for the unknown coefficients and then calculate the corresponding optical fields and the carrier density.

4.1　Photon Density

The output power of the laser is proportional to the intracavity photon density s, which is related

to the optical field as

$$s = s_0 + \left(s_1 e^{-i\hat{\Omega}_0 \tau} + \text{c.c.} \right) + \text{higher harmonics} = x^2 + y^2, \qquad (4.1)$$

where s_0 is the average photon density and s_1 is the amplitude of the photon density oscillating at

the P1 frequency, c.c. denotes the complex conjugate. Figure 4.1 presents the map of the average

photon density s_0 with $m = 2$, which can be expressed as

$$\begin{aligned}
s_0 &= x_0^2 + \frac{1}{2} x_{1o}^2 + \frac{1}{2} x_{1e}^2 + \frac{1}{2} x_{2o}^2 + \frac{1}{2} x_{2e}^2 \\
&\quad + y_0^2 + \frac{1}{2} y_{1o}^2 + \frac{1}{2} y_{1e}^2 + \frac{1}{2} y_{2o}^2 + \frac{1}{2} y_{2e}^2.
\end{aligned} \qquad (4.2)$$

The results from our analysis (red squares) are in good agreement with those from the

numerical simulation (black curves) even in the area near the P2 dynamics region. In the

stable-locking region below the Hopf bifurcation line, our results also agree with the numerical

results. This is straightforward because in this region the oscillating terms of the optical field and

carrier density all vanish; thus our solution degenerates to the steady-state solution of the

stable-locking condition. From (2.14) and (2.15), we can also see that the average optical field

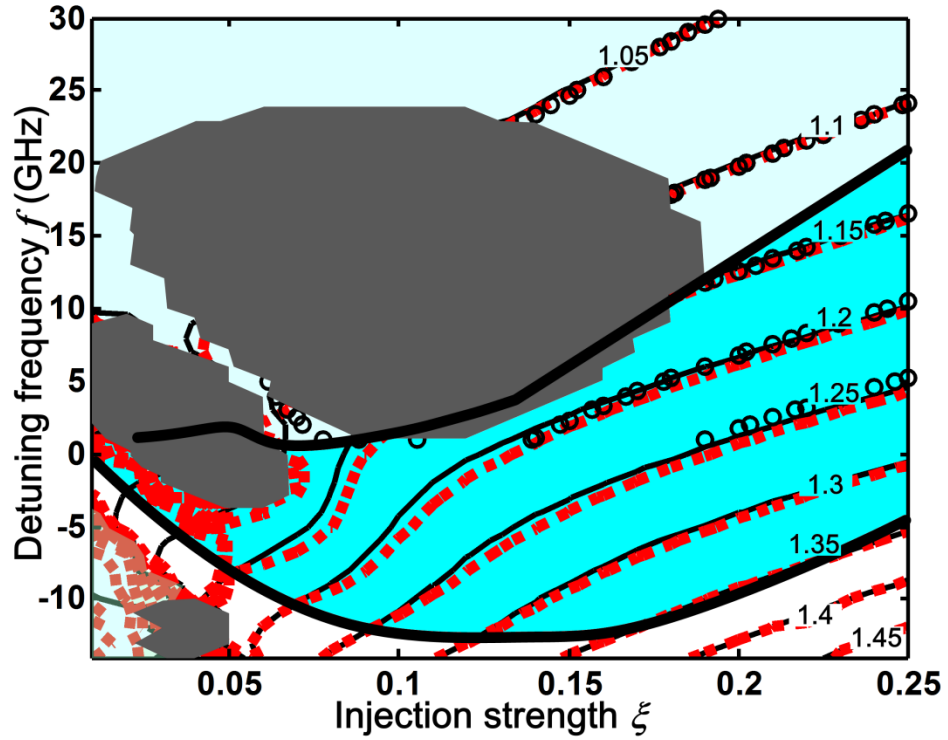amplitudes x_0 and y_0 are proportional to ξ.

Figure 4.1: Average photon density map as a function of optical injection strength and detuning frequency at $\tilde{J} = 1.222$. The contour curves are obtained from our harmonic analysis with $m = 2$ (red squares), the numerical simulation (black curves) and the two-frequency approximation (open circles). The boundary curves and regions separated by them are the same as those described in Fig. 1.1.

However, the average photon density shown in Fig. 4.1 is not simply proportional to ξ^2 because the oscillating terms of the optical field amplitudes also contribute to it. The results from the two-frequency approximation (open circles) are also shown for comparison. It is seen that the two-frequency approximation gives a good estimation except in the highly nonlinear region. The small discrepancy between the results from our analysis and those from the numerical simulation in the highly nonlinear P1 region implies that the nonlinearity is mostly caused by the coupling among the oscillating terms.

In our harmonic analysis, the oscillating amplitude of the optical field is used in the derivation. Experimentally, the microwave signal power measured by a photodetector is proportional to the square of the oscillating laser output power, which is proportional to $|s_1|^2$ given by

$$
\begin{aligned}
|s_1|^2 = &\frac{1}{4}\left(2x_0 x_{1o} - x_{1o}x_{2e} + x_{1e}x_{2o} + 2y_0 y_{1o} - y_{1o}y_{2e} + y_{1e}y_{2o}\right)^2 \\
&+ \frac{1}{4}\left(2x_0 x_{1e} + x_{1o}x_{2o} + x_{1e}x_{2e} + 2y_0 y_{1e} + y_{1o}y_{2o} + y_{1e}y_{2e}\right)^2 .
\end{aligned}
\tag{4.3}
$$

The microwave power map is shown in Fig. 4.2. The results from our analysis with $m = 2$ (red squares) are compared to those from the numerical simulation (black line) and the two-frequency approximation (open circles). Figure 4.2 shows that in the highly nonlinear region the two-frequency approximation completely fails to predict the microwave power. In this region, the oscillating field is stronger than the second-harmonic model predicts. From (2.10), we can
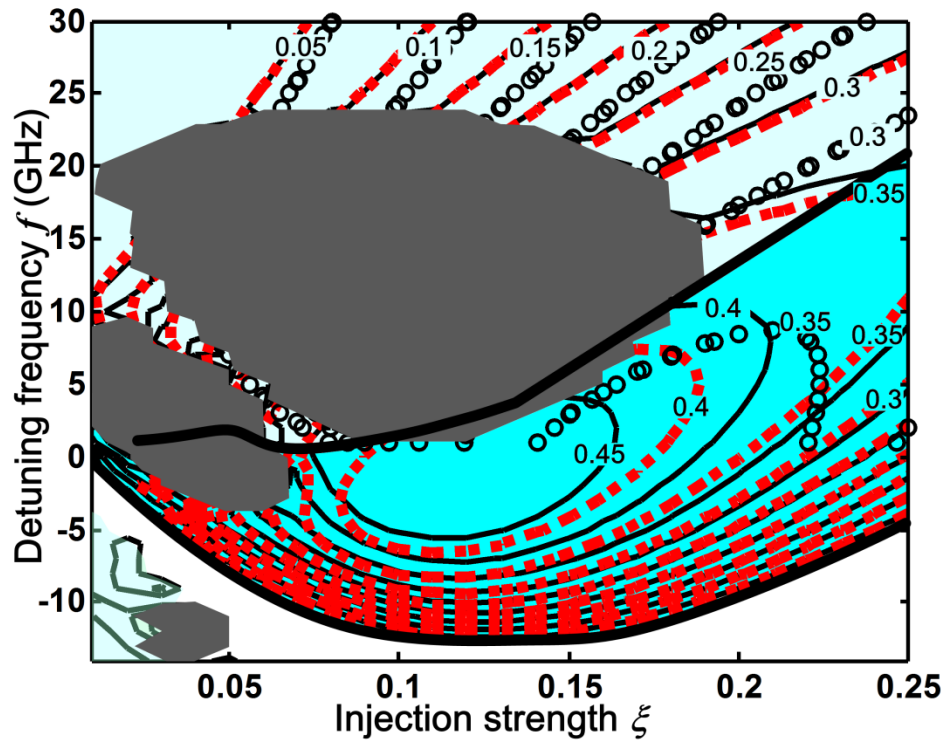
Figure 4.2: Microwave power map as a function of optical injection strength and detuning frequency at $\tilde{J} = 1.222$. The contour curves are obtained from our harmonic analysis with $m = 2$ (red squares), the numerical simulation (black curves) and the two-frequency approximation (open circles). The boundary curves and regions separated by them are the same as those described in Fig. 1.1.

see that the amplitudes of the oscillating optical field components are related to the average optical field components are related to the average optical field amplitudes, x_0 and y_0, and the oscillating carrier density z_1. Because x_0 and y_0 generally decrease with a more positive Ω or a smaller ξ, the behavior of the oscillating optical field is more influenced by z_1.

Figure 4.2 can be divided into two P1 regions by the boundary curve given in (2.23): the upper part is the less nonlinear P1 region, and the lower part is the highly nonlinear P1 region. In the less nonlinear P1 region, Ω is generally large compared to Ω_r. In this region $|s_1|^2$ increases with ξ but is still smaller than its values in the highly nonlinear P1 region. This also implies that the less positive Ω in the highly nonlinear P1 region than those in the less nonlinear region result in a larger amplitude of the oscillating carrier density $|z_1|$. In the highly nonlinear P1 region, the increase of x_0 and y_0 close to the Hopf bifurcation line results in a decrease in z_0 because of the gain deficit due to stimulated emission. Between the Hopf bifurcation line and the boundary curve of (2.23), the injection is strong enough to cause the system to behave highly nonlinearly. Therefore, the largest amplitude of the oscillating carrier density $|z_1|$ and the largest amplitudes of the optical field components are found in an area of a less positive Ω and an intermediate ξ. With the understanding that the microwave power $|s_1|^2$ is proportional to the amplitude of the oscillating optical field components as shown in (4.3), the location of its maximum seen in Fig. 4.2 can be expected.

4.2 Carrier Density

The normalized carrier density is related to z by

$$\tilde{n} = \tilde{n}_0 + \left(\tilde{n}_1 e^{-i\hat{\Omega}_0 \tau} + \text{c.c.}\right) + \text{higher harmonics} = \frac{2\gamma_s \tilde{J}}{\gamma_n}(1+z)$$

$$= \frac{2\gamma_s \tilde{J}}{\gamma_n}\left[(1+z_0) + z_1 \cos\hat{\Omega}_0 \tau\right].$$

$$(4.4)$$

The average carrier density, $\tilde{n}_0$, obtained from our analysis is presented in Fig. 4.3. It shows that in the stable-locking region, the average carrier density $\tilde{n}_0$ decreases with increasing ξ, as expected. It is known that the optical injection can reduce the laser threshold; hence $\tilde{n}_0$ is reduced. However, in the region of P1 dynamics, a significant part of gain is shared by the oscillating P1 harmonic fields. This means that the gain for the average optical field decreases and the threshold reduction becomes less significant. As a result, the average carrier density is clamped at a higher level than that in the stable-locking case.

In Fig. 4.4, the amplitude of the normalized oscillating carrier density, $|\tilde{n}_1|$, is shown. As can be seen in (4.4), $|\tilde{n}_1|$ is directly proportional to $|z_1|$. As discussed above for Fig. 4.2, $|s_1|^2$ increase with $|z_1|$. Consequently, the microwave power $|s_1|^2$ and the oscillating carrier density $|\tilde{n}_1|$ have similar characteristics as functions of detuning frequency and injection strength. This relationship is seen by comparing Fig. 4.2 and 4.4: Both $|\tilde{n}_1|$ and $|s_1|^2$ gradually increase when both Ω and ξ are decreased to a relatively low level.
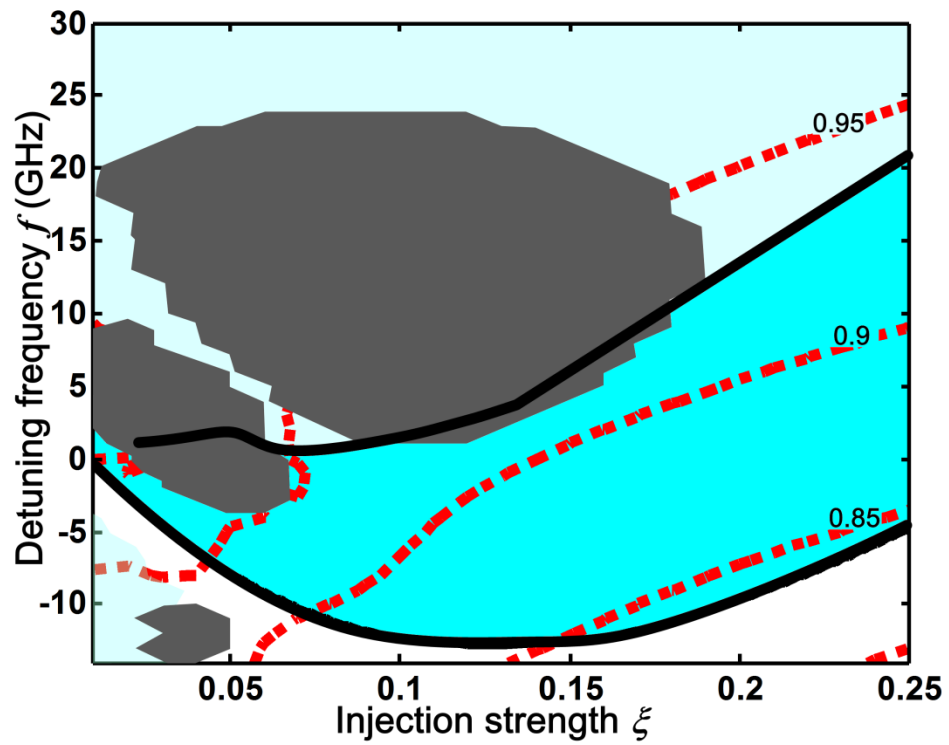
Figure 4.3: Average carrier density as a function of optical injection strength and detuning frequency at $\tilde{J} = 1.222$. The boundary curves and the regions separated by them are the same as those described in Fig. 1.1.

The P1 frequency predicted by the two-frequency approximation is assumed to be the beating between the detuning frequency and the shifted cavity resonance frequency as expressed in (2.9). From Fig. 4.3, it can be seen that above the boundary curve of (2.23) $\tilde{n}_0$ increases with the detuning frequency such that z_0 actually increases to a small value close to zero. The resultant P1 frequency is thus close to the detuning frequency, as expected. By contrast, when the oscillating term is large as in the region bounded by curve of (2.23) and the Hopf bifurcation line, the two-frequency approximation is no longer valid. Although the amplitude of the oscillating term only doubles in strength from the outskirt of the highly nonlinear P1 region to the center, its influence is much more significant than that because of the high nonlinearity, as can be seen from (2.14) and (2.15) which have terms of z_1 to the fourth power.

4.3 Summary

From the calculated photon density and the carrier density, it is shown that the oscillating terms are strongly coupled. The effects of the average terms are less significant on the change of nonlinearity of P1 as compared with the oscillating terms. The gradients of the oscillating terms on both maps points to similar directions. In the region near the Hopf bifurcation line, the large discrepancy between the numerical simulation and the two-frequency approximation shows that the P1 dynamics exhibit higher nonlinearity than in the region above the boundary curve of
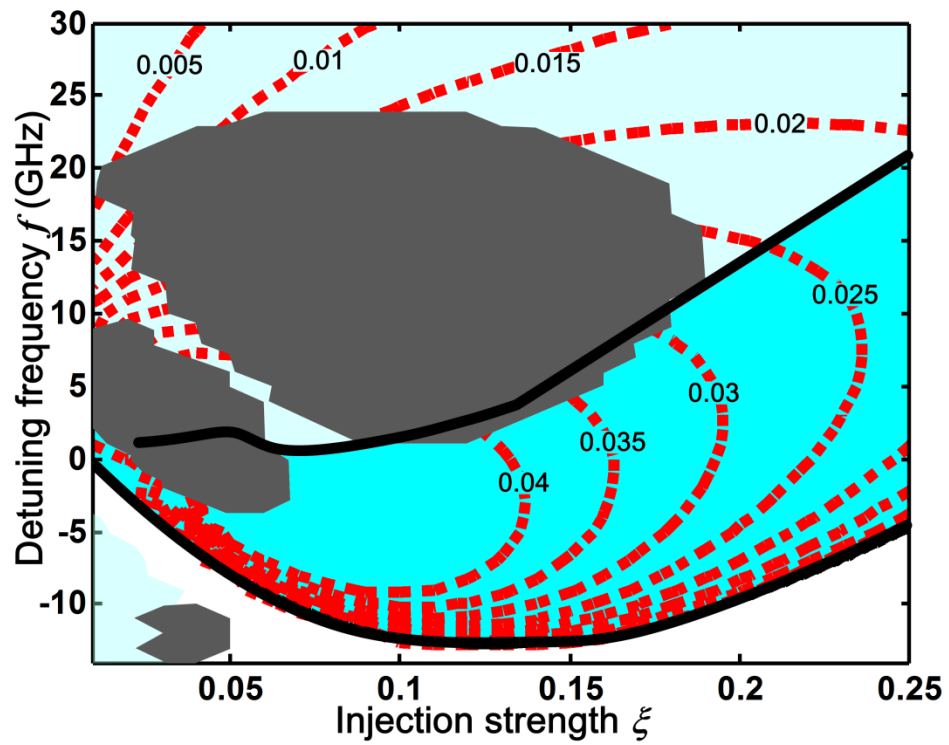
Figure 4.4: Amplitude of the oscillating carrier density as a function of optical injection strength and detuning frequency at $\tilde{J} = 1.222$. The boundary curves and the regions separated by them are the same as those described in Fig. 1.1.

(2.23). This strong coupling is also shown from the derivation of the approximate solution. The

contour shape of the oscillating terms also implies that similar effect should be observed in

optical spectrum, such as sideband ratio.

Chapter 5

Conclusion

5.1 Summary

This thesis illustrates the harmonic analysis of the P1 dynamics of an optically injected semiconductor laser. This approach is based on the general solution form of a limit cycle. The rate equations are solved by balancing the coefficients of the self-consistent solutions. Our analysis starts from the first harmonic of the P1 frequency, and it shows that the first-harmonic optical fields are strongly coupled with the oscillating carrier density. This observation implies that the typical P1 frequency of an optically injected semiconductor laser is not just the beating between the regenerative injection frequency and the shifted cavity resonance frequency.

We also demonstrate that by including up to the third harmonic, we can get excellent

agreement between the analytical and numerical solutions. In addition, our analysis reveals the importance of the second harmonic of the optical field, which must be included to give a good approximation. In contrast, the second harmonic of the carrier density is less important. The strong coupling between the amplitude of the optical field and the first harmonic of the oscillating carrier density is corroborated by the numerical simulation. The maps show that the regions where these oscillating terms dominate are largely overlapped. They also show that a boundary curve exists between the region of relatively low nonlinearity where the two-frequency approximation is useful and the region of high nonlinearity where the harmonics of the P1 frequency must be considered so that the two-frequency approximation completely fails. When the detuning frequency Ω is higher than the resonance frequency Ω_r, the regenerative injection optical field is strong and the two-frequency approximation can be applied. When Ω is lower and ξ is strong, the system easily degenerates into the stable-locking region. In between, when the injection is not strong enough to lock the resonance frequency and the injection optical frequency is not far from the cavity resonance frequency, the P1 oscillation arises from the strong coupling between the oscillating carrier density and the optical fields. In this region, the two-frequency approximation fails whereas our harmonic analysis still yields accurate results. The accuracy further improves when higher harmonic terms are included in the analysis, if necessary.

5.2   Future Research

This thesis provides the analytical approach to solving the coupled nonlinear differential equations for the P1 dynamics. Many P1 characteristics can be investigated through this approach including the noise performance, the optical spectrum and the effect of the linewidth enhancement factor b and the gain saturation factor b'. It is expected that the P1 dynamics in the highly nonlinear region can exhibit sophisticated characteristics. Low-sensitivity point [41] is one of the important application. The sidebands in the optical spectrum are affected by the operation parameters and should be predictable through the similar procedure calculating the oscillating photon density terms. Calculating the sideband ratio could have important application in the signal modulation of the communication system using P1 dynamics for microwave signal generation. Finally, this model can also help to design the values of the intrinsic parameters, such as b and b', for the optimal operation.

Bibliography

[1]   R. Lang and K. Kobayashi. External optical feedback effects on semiconductor injection laser properties. *IEEE J. Quantum Electron*., 16:347-355, 1980.

[2]   J. Mork, B. Tromborg, and J. Mark. Chaos in semiconductor lasers with optical feedback: theory and experiment. *IEEE J. Quantum Electron*., 28:93-108, 1992.

[3]   S. Tang and J.-M. Liu. Chaotic pulsing and quasi-periodic route to chaos in a semiconductor laser with delayed opto-electronic feedback. *IEEE J. Quantum Electron*., 37:329-336, 2001.

[4]   J. S. Lawrence and D. M. Kane. Nonlinear dynamics of a laser diode with optical feedback systems subject to modulation. *IEEE J. Quantum Electron*., 38:185-192, 2002.

[5]   R. Vicente, J. Mulet, C. R. Mirasso, S. Tang and J.-M. Liu. Dynamical properties of semiconductor lasers subject to optoelectronic feedback and bidirectional coupling. *in Quantum Electronics Conference*, *European*, 2003, p. 41.

[6]   F. Y. Lin and J.-M. Liu. Nonlinear dynamics of a semiconductor laser with delayed negative optoelectronic feedback. *IEEE J. Quantum Electron.*, 39:562-568, 2003.

[7]   E.-K. Lee, H.-S. Pang, J.-D. Park, and H. Lee. Bistability and chaos in an injection-locked semiconductor laser. *Phys. Rev. A*, 47:736-739, 1993.

[8]   L. Linlin. A unified description of semiconductor lasers with external light injection and its application to optical bistability. *IEEE J. Quantum Electron.*, 30:1723-1731, 1994.

[9]   T. Erneux, V. Kovanis, A. Gavrielides, and P. M. Alsing. Mechanism for period-doubling bifurcation in a semiconductor laser subject to optical injection. *Phys. Rev. A*, 53:4372-4380, 1996.

[10]   S. Wieczorek, B. Krauskopf, and D. Lenstra. A unifying view of bifurcations in a semiconductor laser subject to optical injection. *Optics Comm.*, 172:279-295, 1999.

[11]   S. Eriksson. Dependence of the experimental stability diagram of an optically injected semiconductor laser on the laser current. *Optics Comm.*, 210:343-353, 2002.

[12]   S. Wieczorek, T. B. Simpson, B. Krauskopf, and D. Lenstra. Bifurcation transitions in an optically injected diode laser: theory and experiment. *Optics Comm.*, 215:125-134, 2003.

[13]   S. Kobayashi and T. Kimura. Injection locking characteristics of an AlGaAs semiconductor laser. *IEEE J. Quantum Electron.*, 16:915-917, 1980.

[14]   R. Lang. Injection locking properties of a semiconductor laser. *IEEE J. Quantum*

Electron., 18:976-983, 1982.

[15]   F. Mogensen, H. Olesen, and G. Jacobsen. Locking conditions and stability properties for

a semiconductor laser with external light injection. *IEEE J. Quantum Electron.*,

21:784-793, 1985.

[16]   I. Petitbon, P. Gallion, G. Debarge, and C. Chabran. Locking bandwidth and relaxation

oscillations of an injection-locked semiconductor laser. *IEEE J. Quantum Electron.*,

24:148-154, 1988.

[17]   T. B. Simpson, J.-M. Liu, and A. Gavrielides. Bandwidth enhancement and broadband

noise reduction in injection-locked semiconductor lasers. *IEEE Photon. Technol. Lett.*,

7:709-711, 1995.

[18]   J.-M. Liu, H.-F. Chen, X. J. Meng, and T. B. Simpson. Modulation bandwidth, noise, and

stability of a semiconductor laser subject to strong injection locking. *IEEE Photon.

Technol. Lett.*, 9:1325-1327, 1997.

[19]   V. Kovanis, A. Gavrielides, T. B. Simpson, and J.-M. Liu. Instabilities and chaos in

optically injected semiconductor lasers. *Appl. Phys. Lett.*, 67:2780-2782, 1995.

[20]   T. B. Simpson, J.-M. Liu, A. Gavrielides, V. Kovanis, and P. M. Alsing. Period-doubling

cascades and chaos in a semiconductor laser with optical injection. *Phys. Rev. A*,

51:4181-4185, 1995.

[21] T. B. Simpson, J.-M. Liu, K.-F. Huang, and K. Tai. Nonlinear dynamics induced by external optical injection in semiconductor lasers. *Quantum and Semiclassic. Opt.*, 9:765, 1997.

[22] B. Krauskopf, N. Tollenaar, and D. Lenstra. Tori and their bifurcations in an optically injected semiconductor laser. *Optics Comm.*, 156:158-169, 1998.

[23] S.-K. Hwang and J.-M. Liu. Dynamical characteristics of an optically injected semiconductor laser. *Optics Comm.*, 183:195-205, 2000.

[24] A. Gavrielides, V. Kovanis, M. Nizette, T. Erneux, and T. B. Simpson. Period three limit-cycles in injected semiconductor lasers. Quantum and Semiclassic. Opt., 4:20, 2002.

[25] S. Wieczorek, T. Simpson, B. Krauskopf, and D. Lenstra. Global quantitative predictions of complex laser dynamics. *Phy. Rev. E*, 65:045207, 2002.

[26] T. B. Simpson. Mapping the nonlinear dynamics of a distributed feedback semiconductor laser subject to external optical injection. *Optics Comm.*, 215:135-151, 2003.

[27] S.-K. Hwang, J.-M. Liu, and J. K. White. Characteristics of period-one oscillations in semiconductor lasers subject to optical injection. *IEEE J. Selec. Topics in Quantum Electron.*, 10:974-981, 2004.

[28] S. Wieczorek and B. Krauskopf. Bifurcations of n-homoclinic orbits in optically injected lasers. *Nonlinearity*, 18:1095-1120, 2005.

[29] S.-C. Chan, R. Diaz, and J.-M. Liu. Novel photonic applications of nonlinear semiconductor laser dynamics. *Optic. and Quantum Electron.*, 40:83-95, 2007.

[30] S.-C. Chan and J.-M. Liu. Frequency modulation on single sideband using controlled dynamics of an optically injected semiconductor laser. *IEEE J. Quantum Electron.*, 42:699-705, 2006.

[31] S.-C. Chan, S.-K. Hwang, and J.-M. Li,. Radio-over-fiber AM-to-FM upconversion using an optically injected semiconductor laser. *Optics Lett.,* 31:2254-2256, 2006.

[32] F.-Y. Lin and J.-M. Liu. Chaotic lidar. *IEEE J. Selec. Topics in Quantum Electron.*, 10:991-997, 2004.

[33] R. Diaz, S.-C. Chan, and J.-M. Liu. Lidar detection using a dual-frequency source. *Optics Lett.,* 31:3600-3602, 2006.

[34] T. Fordell and Å. M. Lindberg. Numerical stability maps of an optically injected semiconductor laser. *Optics Comm.,* 242:613-622, 2004.

[35] S. Wieczorek, B. Krauskopf, T. B. Simpson, and D. Lenstra. The dynamical complexity of optically injected semiconductor lasers. *Phys. Reports,* 416:1-128, 2005.

[36] S.-C. Chan. Analysis of an Optically Injected Semiconductor Laser for Microwave Generation. *IEEE J. Quantum Electron.*, 46:421-428, 2010.

[37] S. Liao. On the homotopy analysis method for nonlinear problems. *Appl. Mathematics*

and Computation, 147:499-513, 2004.

[38]   M. Ganjiani and H. Ganjiani. Solution of coupled system of nonlinear differential equations using homotopy analysis method. *Nonlinear Dynamics,* 56:159-167, 2009.

[39]   J.-H. He. Variational iteration method for autonomous ordinary differential systems. *Appl. Mathematics and Computation,* 114:115-123, 2000.

[40]   A. Barari, M. Omidvar, A. Ghotbi, and D. D. Ganji. Application of Homotopy Perturbation Method and Variational Iteration Method to Nonlinear Oscillator Differential Equations. *Acta Applicandae Mathematicae,* 104:161-171, 2008.

[41]   T. B. Simpson, J.-M. Liu, M. AlMulla, N. G. Usechak, and V. Kovanis. Limit-Cycle Dynamics with Reduced Sensitivity to Perturbations. *Phys. Rev. Lett.,* 112:023901, 2014.

[42]   T. B. Simpson, J.-M. Liu, and A. Gavrielides. Small-signal analysis of modulation characteristics in a semiconductor laser subject to strong optical injection. *IEEE J. Quantum Electron.,* 32:1456-1468, 1996.

[43]   S.-C. Chan, S.-K. Hwang, and J.-M. Liu. Period-one oscillation for photonic microwave transmission using an optically injected semiconductor laser. *Optics Express,* 15:14921-14935, 2007.

[44]   J.-M. Liu and T. B. Simpson. Four-wave mixing and optical modulation in a semiconductor laser. *IEEE J. Quantum Electron.,* 30:957-965, 1994.

[45] S.-K. Hwang, J.-M. Liu, and J. K. White. 35-GHz intrinsic bandwidth for direct modulation in 1.3-μm semiconductor lasers subject to strong injection locking. *IEEE Photon. Technol. Lett.,* 16:972-974, 2004.

[46] J.-H. He. Determination of Limit Cycles for Strongly Nonlinear Oscillators. *Phys. Rev. Lett.,* 90:174301, 2003.

[47] J.-H. He. Limit cycle and bifurcation of nonlinear problems. *Chaos, Solitons & Fractals,* 26:827-833, 2005.

[48] T. B. Simpson and J.-M. Liu. Enhanced modulation bandwidth in injection-locked semiconductor lasers. *IEEE Photon. Technol. Lett.,* 9:1322-1324, 1997.

[49] A. Murakami, K. Kawashima, and K. Atsuki. Cavity resonance shift and bandwidth enhancement in semiconductor lasers with strong light injection. *IEEE J. Quantum Electron.*, 39:1196-1204, 2003.

[50] M. AlMulla and J.-M. Liu. Effects of the Gain Saturation Factor on the Nonlinear Dynamics of Optically Injected Semiconductor Lasers. *IEEE J. Quantum Electron.*, 50:158-165, 2014.